Catalysis Today 152 (2010) 33–41

Contents lists available at ScienceDirect

Catalysis Today

journal homepage: www.elsevier.com/locate/cattod

Meso–macroporous zirconia modified with niobia as support for platinum—Acidic and basic properties

Joanna Goscianska [a], Maria Ziolek [a,*], Emma Gibson [b], Marco Daturi [b]

[a] Adam Mickiewicz University, Faculty of Chemistry, Grunwaldzka 6, 60-780 Poznań, Poland
[b] Laboratoire Catalyse et Spectrochimie, UMR 6506 – CNRS, ENSICaen and Université de Caen Basse-Normandie, 6, Boulevard du Maréchal Juin, 14050 Caen Cedex, France

ARTICLE INFO

Article history:
Available online 28 November 2009

Keywords:
Niobio-zirconia
Supports for platinum
Structure/texture
Acid–base properties

ABSTRACT

Meso–macroporous tetragonal zirconia synthesised hydrothermally within this work and containing ca. 60% of mesopores and a surface area of 84 m^2/g is a highly basic material exhibiting both Brønsted and Lewis basicities (BBS and LBS). Moreover, it has Lewis acid sites and very weak BAS (bridged hydroxyls). Such ZrO_2 was used as a matrix for niobium oxide species loaded as 0.3 and 1 monolayers. NbOx loading decreases basicity (both LBS and BBS) and the number of Lewis acid sites (LAS) and leads to an increase in the number of Brønsted acid sites (BAS). The loading with a 0.3 monolayer of NbOx leads to a very attractive support/catalyst because of the generation of active oxygen atoms at the interface between the NbOx and ZrO_2 phases. Niobio-zirconia supports were modified by impregnation with chloroplatinic acid (1 wt% of Pt). Platinum modification further changes the acid–base properties of the supports, depending on the NbOx loading. The highest Pt dispersion is reached on the NbOx monolayer because of the strong metal–support interaction. Structure and surface properties (acid–base) of the supports and platinum catalysts were characterized in detail by N_2 adsorption, XRD, XPS, UV–vis, FTIR combined with the adsorption of probe molecules (pyridine, CO at room temperature and ~100 K, CO_2), and by test reactions (acetonylacetone cyclization and 2-propanol dehydration/dehydrogenation).

1. Introduction

Zirconia is an amphoteric substance being able to show both mildly acidic and basic properties, which can be converted into a strong acid. Therefore, zirconia is a promising support material and can be used as catalyst by itself. The ability of any catalyst support to sustain a high surface area under demanding conditions is very important. In our previous studies we have used mesoporous MCM-41 materials with very high surface areas as supports for Zr species [1,2]. In this work our focus was on mesoporous zirconia with relatively high surface area prepared according to [3,4].

Niobium-containing catalysts appear to be attractive for both gas phase and liquid phase reactions (e.g. [5,6]). Among them niobium oxide is known as a material strongly interacting with metals (responsible for strong metal–support interaction—SMSI) and it reveals acidic and redox properties depending on the support on which it is loaded.

The combination of zirconia and niobia could give rise to interesting catalysts and/or supports for noble metals. The literature devoted to niobio-zirconia binary systems is rather modest (e.g. [7,8]). According to our best knowledge there is no data published on the use of these binary oxides as supports for platinum. Thus, the idea of this work was to obtain three supports for platinum based on pure mesoporous ZrO_2, and zirconia modified with NbOx species (0.3 and 1 monolayers loading of niobium oxide). One monolayer of NbOx can obstruct access to the zirconia surface by the platinum source and reagents in catalytic reactions, whereas the 0.3 monolayer of NbOx leaves a large part of the zirconia surface free for interaction with the platinum precursor and reagents in the reaction. Moreover, one can expect the diversity in the acid and basic properties, depending on niobium loading, to determine the behaviour of platinum loaded on such supports. The catalysts prepared have been tested in redox processes (DeNOx, WGS) not reported here. This work deals with the synthesis and detailed characterization of structure and surface properties of ZrO_2–NbOx and Pt modified materials. Various complementary methods used for the characterization allowed a deep insight into the acid–base properties, reported in this paper.

2. Experimental

2.1. Catalyst preparation

For the preparation of meso–macroporous zirconia a typical procedure described in Refs. [3,4] was used. A 15 wt% micellar

* Corresponding author. Tel.: +48 61 8291243; fax: +48 61 829 1505.
E-mail addresses: ziolek@amu.edu.pl (M. Ziolek), Marco.Daturi@ensicaen.fr (M. Daturi).

0920-5861/$ – see front matter © 2009 Elsevier B.V. All rights reserved.
doi:10.1016/j.cattod.2009.10.016

solution of cetyltrimethylammonium bromide (CTMABr) was prepared by dissolving CTMABr (Aldrich) in an aqueous acidic solution (HCl, pH 2) at 313 K while stirring for a minimum of 3 h. An appropriate quantity of zirconium propoxide ($Zr(OC_3H_7)_4$) was added dropwise into the above solution at the surfactant/Zr molar ratio of 0.33. After further stirring for 1 h at room temperature, the mixture was transferred into a polypropylene bottle, and heated in an oven at 333 K for 48 h. The sample was calcined in air at 673 K for 4 h.

$NbOx/ZrO_2$ samples were prepared by incipient wetness impregnation of ZrO_2 with trisoxalate ammonium complex of niobium (CBMM, Brazil). Nb surface densities were calculated on the basis of the surface area of the zirconia support (84 m^2/g). The nominal monolayer coverage was calculated assuming that the cross-section of Nb_2O_5 unit occupies a surface of 0.32 nm^2 [9]. The solids were then dried at 373 K for 5 h and calcined in air for 5 h at 673 K.

Incipient wetness technique was used to impregnate all the materials with an aqueous solution of hexachloroplatinic acid ($H_2PtCl_6{\cdot}H_2O$, Aldrich) in the amount necessary to obtain 1 wt% Pt loading. The catalysts were successively dried at 373 K for 5 h (temperature ramp 12 K min^{-1}) and calcined in air for 3 h at 673 K (temperature ramp 2 K min^{-1}) and reduced in 5% $H_2 + N_2$ flow at 773 K for 3 h.

2.2. Catalyst characterization

The prepared materials were characterized by X-ray diffraction (XRD) using a D8 Advance diffractometer (Bruker) (CuK_α radiation, $\lambda = 0.154$ nm).

Surface areas, pore diameters and pore volumes of the samples were calculated from low-temperature nitrogen adsorption isotherms measured on a Micromeritics 2010 sorptometer. Prior to adsorption measurements, the samples were degassed in vacuum at 573 K for 3 h.

TEM and SEM studies were performed using a JEOL 2000 electron microscope operating at 80 and 15 kV, respectively. Powdered samples were deposited on a grid with a holey carbon film before being transferred to the electron microscope.

UV–vis spectra were recorded using a Varian-Cary 300 Scan UV–vis spectrophotometer. Catalyst powders were placed into the cell equipped with a quartz window. The Kubelka–Munk function ($F(R)$) was used to convert reflectance measurements into equivalent absorption spectra using the reflectance of SPECTRALON as a reference.

The oxidation state of the metals was estimated from XPS measurements which were performed on a VSW apparatus (Vacuum Systems Workshop Ltd., England).

Platinum dispersion was estimated by hydrogen chemisorption combined with measurements on a Micromeritics 2010 sorptometer. The following procedure was applied in the measurements: preliminary evacuation and heating at 573 K for 1 h, the flow of hydrogen at 573 K for 1 h, evacuation at 573 K for 2 h, cooling down to 308 K, leak test and finally the measurement of hydrogen uptake at 308 K.

Moreover, dispersion of platinum was calculated from FTIR spectra of CO adsorbed at room temperature (Nicolet Magna 550 FTIR spectrometer) using self supported discs of samples (10 mg cm^{-2}) placed in the classical quartz cell. Prior to the adsorption, the samples were treated three times with hydrogen and vacuum ($\sim 10^{-4}$ Pa) at 573 K for 1.5 h. After which small doses of CO (0.04–7.75 μmol) were admitted and the spectra were measured.

2.3. Acidity–basicity measurements

The catalysts were tested for acetonylacetone (AcAc) cyclization and 2-propanol (2-PrOH) decomposition as probe reactions. A tubular, down-flow reactor was used for the AcAc cyclization reaction which was carried out at atmospheric pressure, using nitrogen as the carrier gas. The catalyst bed (0.05 g) was first activated for 2 h at 673 K under nitrogen flow (40 cm^3 min^{-1}). Subsequently, a 0.5 cm^3 of acetonylacetone (Fluka, GC grade) was passed continuously over the catalyst at 623 K. The substrate was delivered with a pump system and vaporized before being passed through the catalyst with a flow of nitrogen carrier gas (40 cm^3 min^{-1}). The reaction products were collected for 30 min downstream of the reactor in a cold trap and analysed by gas chromatography (CHROM-5, Silicone SE-30/Chromosorb column).

The 2-propanol conversion (dehydration and dehydrogenation) was performed using a microcatalytic pulse reactor inserted between the sample inlet and the column of a CHROM-5 chromatograph. The catalyst bed (0.02 g) was first activated at 673 K for 2 h under helium flow (40 cm^3 min^{-1}). The 2-propanol (Aldrich) conversion was studied at 423, 473, 523 and 573 K using 3 μl pulses of alcohol under helium flow (40 cm^3 min^{-1}). The reactant and reaction products: propene, 2-propanone (acetone) and diisopropyl ether were analysed using an online CHROM-5 gas chromatograph. The reaction mixture was separated on a 2 m column filled with Carbowax 400 (80–100 mesh) at 338 K under helium flow (40 cm^3 min^{-1}) and detected by TCD.

Acid–base properties were studied by in situ FTIR spectroscopy of adsorbed probe molecules, using sample wafers of 10 mg cm^{-2} analysed in a classical quartz cell. The spectra were recorded at room temperature with a Nicolet Magna 550 FTIR spectrometer (resolution 4 cm^{-1}) after quenching the samples to room temperature. Probe molecules (CO, CO_2 and pyridine) were introduced at room temperature on the activated samples (activation at 673 K under vacuum) and then evacuated. CO adsorption at ~100 K was also performed after several treatments of the samples with hydrogen. Gas pressure and additional information about operating procedures are reported in the text for each probe. The spectra were treated by the Nicolet OMNIC™ software.

3. Results

3.1. Texture/structure characterization

The catalysts applied in this work and the data calculated from N_2 adsorption isotherms are shown in Table 1. The parent materials are meso–macroporous and exhibit surface areas of about 80 m^2/g. The impregnation of zirconia with niobium salt and chloroplatinic acid only slightly influences the texture features (surface area and pore volume decrease). SEM images indicate a well crystalline material and TEM results reveal well ordered mesopores in all supports used for platinum (SEM and TEM images not shown here).

The X-ray diffraction patterns of all samples are shown in Fig. 1. In the high-angle range the calcined supports (zirconia and

Table 1
Texture parameters of the catalysts.

Catalyst	S_{BET} (m^2/g)	Average pore diameter (nm)	Pore diameter from PSD (nm)[a]	Total volume (cm^3/g)	Mesopore volume (cm^3/g)
ZrO_2	84	5.6	2.7	0.15	0.09
$0.3Nb/ZrO_2$	80	5.5	2.7	0.15	0.08
$1Nb/ZrO_2$	80	5.2	2.5	0.13	0.08
Pt/ZrO_2	79	5.6	2.8	0.15	0.09
$Pt/0.3Nb/ZrO_2$	80	5.4	2.7	0.14	0.08
$Pt/1Nb/ZrO_2$	76	5.3	2.7	0.12	0.08

[a] Estimated from the maximum on PSD curve in mesopore region.

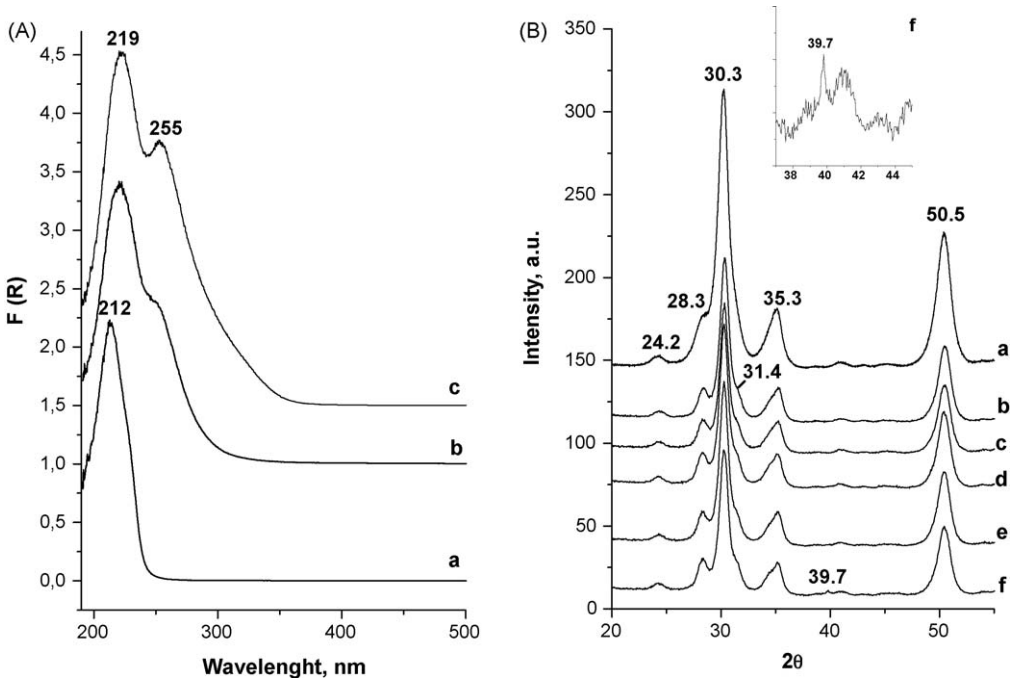

Fig. 1. (A) UV–vis spectra of ZrO_2 (a), 0.3Nb/ZrO_2 (b), 1Nb/ZrO_2 (c) and (B) X-ray diffraction patterns of ZrO_2 (a), 0.3Nb/ZrO_2 (b), 1Nb/ZrO_2 (c), Pt/ZrO_2 (d), Pt/0.3Nb/ZrO_2 (e), Pt/1Nb/ZrO_2 (f).

niobia–zirconia) exhibited mainly the tetragonal phase of zirconia (JCPDS 50-1089) characterized by the peaks at 2θ = 30.3, 35.3 and 50.5°.

Comparison of XRD patterns of ZrO_2 (Fig. 1Ba), 0.3Nb/ZrO_2 (Fig. 2Bb), 1Nb/ZrO_2 (Fig. 1Bc) indicates small changes after NbOx loading. XRD peaks assigned to crystalline niobium oxides are placed in positions similar to those in the ZrO_2 spectrum. Therefore, they are not well distinguished. However, a deep insight into the shape of XRD patterns allow us to find a peak at 28.3° for all niobium-containing samples (Fig. 1Bb–f) better resolved than that obtained in the spectrum of pristine ZrO_2 (Fig. 1Ba). Moreover, a shoulder at 31.4° is present only in XRD patterns of NbOx loaded materials. Thus, one can assign them to the presence of the NbOx crystalline phase on the ZrO_2 support as the positions of these peaks are characteristic of Nb_2O_5 (JCPDS 19-864). The presence of such species is confirmed by the UV–vis study (Fig. 1A). Impregnation with platinum followed by calcination did not change significantly the XRD patterns with the exception of that of Pt/1Nb/ZrO_2, in which one peak from Pt^0 at 39.7° originating from (1 1 1) plane is well seen (Fig. 1Bf) [10].

UV–vis spectra of ZrO_2 showed a band at 212 nm attributed to a charge transfer from O^{2-} to Zr^{4+} ion with tetrahedral configuration (Fig. 1A) [11,12]. Impregnation with niobium species results in a shift of this band towards a higher wavelength (222 nm) indicating the chemical interaction between ZrO_2 and Nb species. Moreover, the band at ~250 nm is observed as one of the two UV bands recorded for Nb_2O_5 [13]. The absence of the second UV band at ~350 nm, which is also characteristic of bulk Nb_2O_5, can suggest the chemical interaction of Nb_2O_5 with ZrO_2 support or isolation of Nb species partially included into the zirconia structure [14].

Cationic accessibility at the surface of solids was estimated from the IR bands of CO adsorbed at room temperature. Fig. 2 shows the spectra (CO stretching region) recorded for all materials after adsorption of incremental doses of the CO probe molecule. For zirconia we found only one type of CO adsorption site (a band at 2195 cm^{-1}), which is characteristic of CO coordinated to cationic sites (Zr^{4+}-CO) on tetragonal zirconia, whereas two coordinatively unsaturated zirconium sites are expected for the monoclinic phase [15]. For NbOx modified samples a band at ~2197 cm^{-1} is observed. It can overlap the bands from CO chemisorbed on both zirconium and niobium cations. Hadjiivanov and Vayssilov [15] infer that at the present state of knowledge an unambiguous determination of the oxidation state of the Nb^{n+} ion on the basis of the IR spectra of adsorbed CO is not possible. The band at 2143 cm^{-1}, visible only at high CO coverage rates, can be assigned to CO in the gas phase. Additionally, the spectra of 0.3Nb/ZrO_2 and 1Nb/ZrO_2 materials reveal the bands characteristic of the products of reactive CO adsorption (in the form of carbonates and hydrogen-carbonates). All these species are characterized by stretching modes below 1700 cm^{-1}. The bands originating from the carbonates on 0.3Nb/ZrO_2 have an intensity which is more than double than those assigned to the carbonates on 1Nb/ZrO_2. Thus, the monolayer of Nb species decreases the activity of carbonate formation in relation to that observed on 0.3Nb/ZrO_2, which suggests that oxygen located in the corner between NbOx crystallites and ZrO_2 support is active in the oxidation of adsorbed CO to carbonates.

Various oxygen species and oxidation states of metals were concluded from XPS results. The binding energies obtained (BEs) are summarized in Table 2. Those for Zr3d are typical of Zr^{4+} in zirconium oxides [16,17] whereas the binding energies of Nb3d in NbOx species impregnated zirconia are a little bit lower than those in the crystalline Nb_2O_5 (207.3 eV) [18]. This behaviour suggests a strong interaction of Nb with the zirconia support. BE of Pt^0 ranges between 70.8 and 71.9 eV, the higher when Nb-impregnated support is used. It is caused by the strong interaction of metallic platinum and NbOx. For Pt/0.3Nb/ZrO_2, a BE of 73.4 eV due to cationic platinum is detected and the band assigned to this species dominates the XPS spectrum (not shown here).

CO adsorption on materials impregnated with platinum was also studied (Fig. 2, right). In the IR spectrum of Pt modified ZrO_2 and 1Nb/ZrO_2, the bands at ~2080 cm^{-1} and ~1850 cm^{-1} assigned to linear and bridging carbonyls of Pt^0 were observed. The presence of Pt^{2+}–CO and Pt^{+}–CO complexes were evidenced by the bands at 2205–2170 cm^{-1} and 2135–2120 cm^{-1}, respectively [15], the former features being partially superimposed to those belonging

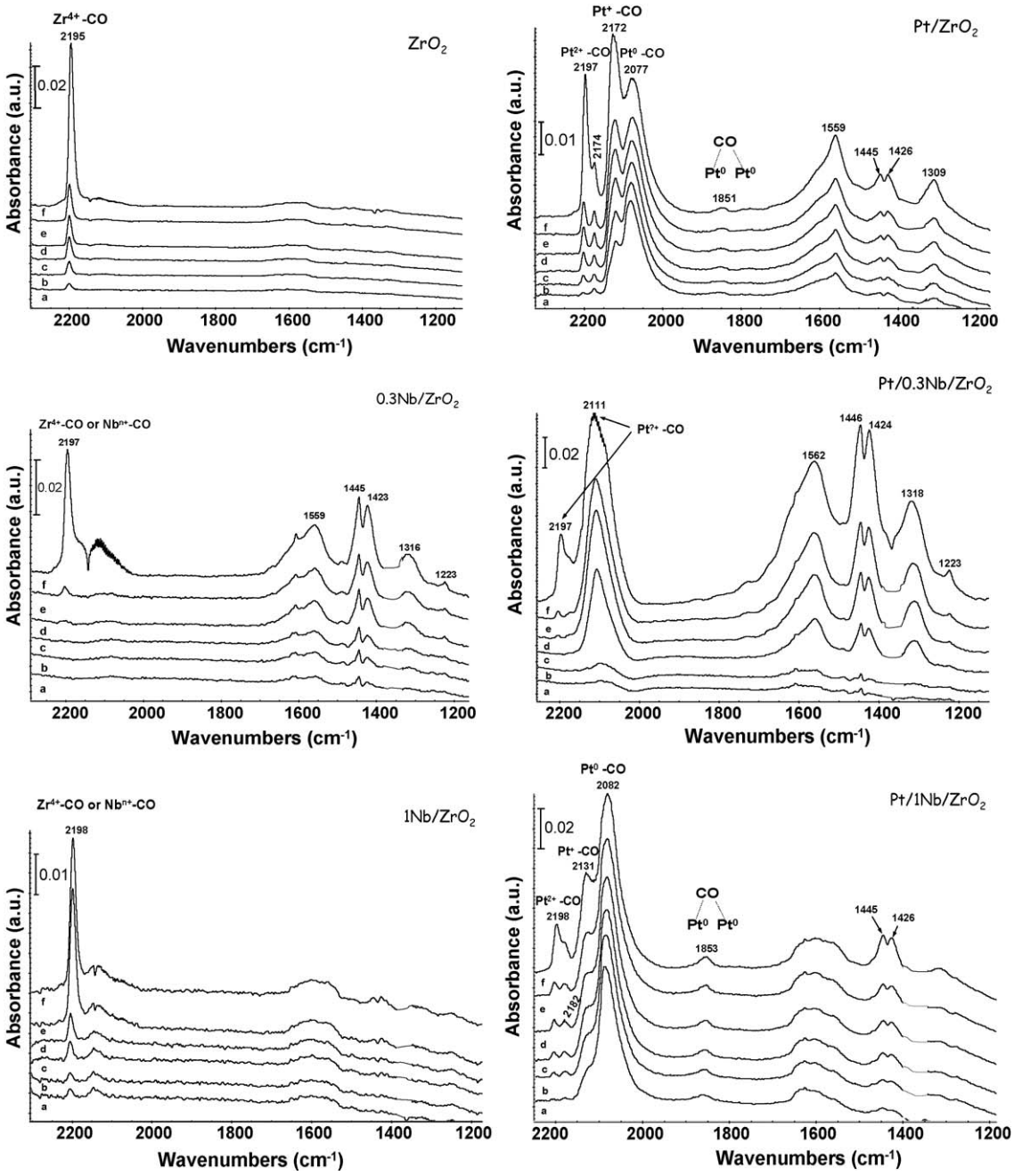

Fig. 2. FTIR spectra of CO adsorbed at room temperature on ZrO_2, 0.3Nb/ZrO_2, 1Nb/ZrO_2, Pt/ZrO_2, Pt/0.3Nb/ZrO_2, Pt/1Nb/ZrO_2. CO concentration was increased from 0.39 to 4.24 μmol (from a to f).

to CO carbonyls on the support. The spectrum of Pt/0.3Nb/ZrO_2 gives no indication of CO adsorbed on metallic platinum. It is in line with the results of the XPS experiments showing the dominance of platinum cationic species.

Pt dispersion on the supports was estimated on the basis of CO adsorption at room temperature, from the curve of the relationship between the area under the IR band from CO adsorbed on the surface and the amount [μmol] of CO/mg on the catalyst [19]. An exemplary curve is shown in Fig. 3. Pt dispersion was also estimated from hydrogen chemisorption. The results obtained by both methods are shown in Table 3. They are in very good agreement.

Meso–macroporous zirconia (60% of mesopores, surface area 84 m^2/g) gives a 75% dispersion of platinum. Interestingly, the 0.3 monolayer of NbOx loaded on ZrO_2 leads to the decrease of Pt dispersion (to 63%), whereas the monolayer of NbOx on ZrO_2 significantly enhances Pt dispersion (to 91%). These results suggest that in the case of binary oxides (Nb and Zr oxides), as supports for platinum, ZrO_2 is the preferential platinum location when a 0.3 of monolayer of NbOx is used. Platinum located on zirconia surface in the holes between NbOx islands agglomerates easily on heating. In contrast, when the monolayer of NbOx is applied, platinum is loaded on niobium oxide and, because of SMSI behaviour of niobium oxides [5], the sintering effect on heating is negligible. Therefore, high dispersion of Pt is reached if NbOx is loaded as a monolayer.

3.2. Acidity and basicity studies

The surface acidity of the support samples was determined by various methods. The adsorption of pyridine measured by FTIR

Table 2
XPS results.

Catalyst	BE (eV)			
	Zr3d	Nb3d	Pt4f	O1s
ZrO_2	181.9 180.1	–	–	529.8 531.4 527.6
$0.3Nb/ZrO_2$	181.8 180.1	206.5 209.2	–	529.6 531.2 527.8
Nb/ZrO_2	181.9 180.1	207.1 212.0	–	529.7 531.4 527.6
Pt/ZrO_2	181.6	–	70.8	529.6 531.2 527.8
$Pt/0.3Nb/ZrO_2$	181.9 180.2	206.7 209.5	71.2 73.4	529.7 531.4 527.9
$Pt/Nb/ZrO_2$	182.1 180.0	206.9	71.9	530.0 531.7 528.0

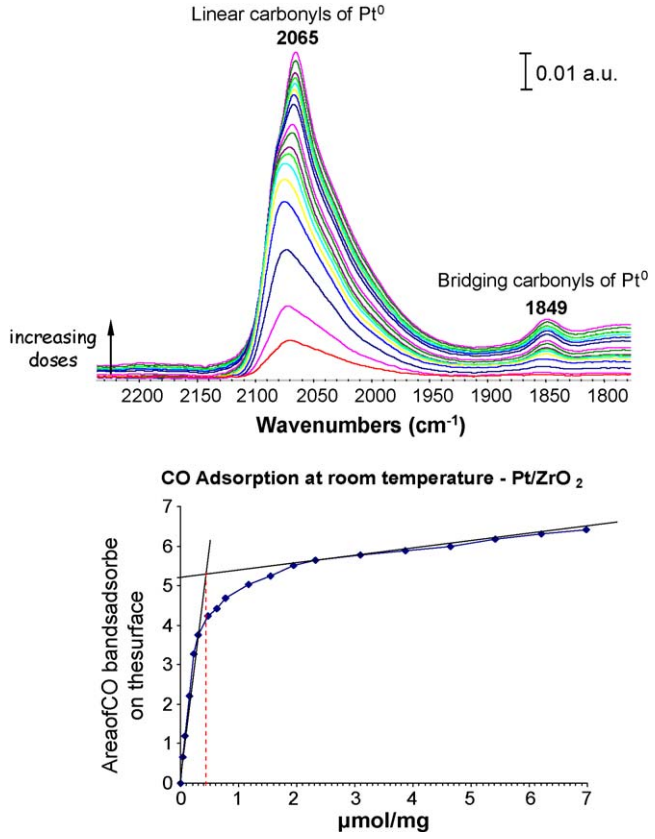

Fig. 3. Spectra of surface reduced Pt/ZrO_2 after CO adsorption (doses from 0.04 to 7.75 μmol) at room temperature and a curve for the calculation of platinum dispersion.

spectroscopy gave information about Lewis and Brønsted acidities [20]. Fig. 4 shows a set of in situ FTIR spectra of pyridine adsorption on all the materials. Lewis acid sites (LAS) are evidenced by the bands at ~1445 and ~1605 cm^{-1}. The intensity of the first one is related to the number of LAS, whereas the position of the second band characterizes the strength of LAS. It is clear that the highest intensity of the band at ~1445 cm^{-1} is observed on pristine ZrO_2.

Table 3
Platinum dispersion calculated from CO adsorption at room temperature and hydrogen chemisorption at 308 K.

Catalyst	Pt dispersion (from CO ads.) (%)	Pt dispersion (from H_2 ads.) (%)	Surface area of Pt (m^2/g)	Average Pt crystallite size (nm)
Pt/ZrO_2	75	77	191	1.5
$Pt/0.3Nb/ZrO_2$	63	60	149	1.9
$Pt/1Nb/ZrO_2$	91	93	230	1.2

The calculation of the number of LAS on the basis of this intensity and extinction coefficient [21] led to the values shown in Table 4. The highest number of LAS was found on ZrO_2. It significantly decreases after NbOx loading suggesting the interaction of Nb species with the LAS on ZrO_2. Platinum loading also causes a decrease in the number of LAS. It is important to stress that the shift of the band ν_{8a} at ca. 1605 cm^{-1} towards higher wavenumbers after NbOx loading indicates the increase in the strength of LAS.

As concerns Brønsted acidity a band at 1546 cm^{-1} (ν_{19b}) assigned to pyridinium cations (and associated to a ν_{8a} mode near 1640 cm^{-1}) is well distinguished only on $Pt/0.3Nb/ZrO_2$ (Fig. 4B). However, one cannot exclude the presence of Brønsted acid sites (BAS) on the other samples containing NbOx species loaded on ZrO_2 because their IR spectra show broad weak bands at this position. But there is no doubt that there are no BAS detected by pyridine adsorption on pristine ZrO_2.

The results described above are not in line with those obtained after low-temperature adsorption of CO on ZrO_2 reported below and shown in Fig. 5 and Table 5. CO adsorption at low temperature (~100 K) can in fact be used to investigate surface acidity, distinguishing between Lewis and Brønsted, weakly interacting acid sites. Two ν(CO) regions can be observed: the first at higher wavenumber (2235–2180 cm^{-1}) due to CO coordination on Lewis acid sites and the second (2180–2150 cm^{-1}) due to adsorption on Brønsted or weak Lewis acid sites. In our case we observe bands in both regions. The feature at lower wavenumber can be assigned to the presence of CO molecules interacting with weak Lewis acid sites, i.e. coordinatively unsaturated Zr^{4+} cations located on extended patches of ZrO_2 crystallites [22], but it might also be due to CO interacted with BAS. Attentively scrutinising spectra, we have observed also changes in the hydroxyl region caused by the adsorption of increasing doses of CO at 100 K, which seems to confirm the presence of Brønsted acid sites, more than the existence of weak Lewis sites. Therefore, we can propose that our results reveal weak BAS on pristine ZrO_2, as already observed by Morterra et al. on parent compounds [23]. Somebody can argue that BAS were hardly detected on zirconia and that the corresponding hydroxyl perturbation described here, after CO adsorption at low temperature, is similar to that observed for silica. But we can mention that also for silica we could somewhat consider the presence of a weak Brønsted acidity, corresponding to a value of the Hammet constant $H_0 = -3$, as recently pointed out when studying the acidity ranking scale of various solids [24]. We should in fact recall that the phenomenon observed by CO adsorption at low temperature is related to the formation of a hydrogen bond, whose variation is continue and proportional to the $\Delta\nu$(OH) shift. It is therefore arbitrary to fix a minimum shift correlated with a "real" Brønsted acidity. It seems to us more correct to talk about weak and strong acidities, depending on the strength of the interaction and on the consequent $\Delta\nu$(OH) shift. A possible explanation of the observed discrepancy between the results given by CO and pyridine probe molecule adsorption is that CO (being a smaller molecule than pyridine) can access a majority of sites located in the porosity of the material, which is not the case for the larger probe [25]. Another reason could be that a decrease in

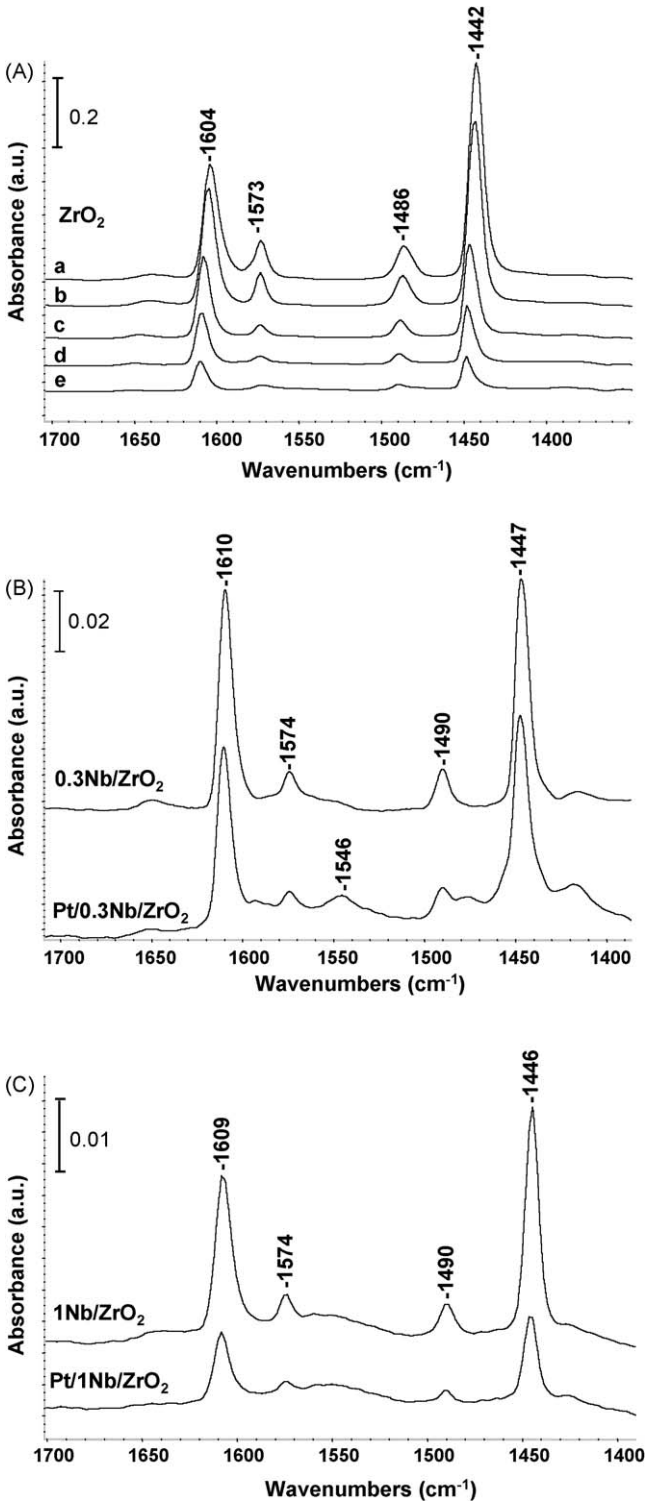

Fig. 4. Spectra of ZrO_2 after pyridine adsorption at RT: A—(a), after evacuation at 323 K (b), 373 K (c), 423 K (d), 473 K (e) and B—0.3Nb/ZrO_2, Pt/0.3Nb/ZrO_2, C—1Nb/ZrO_2, Pt/1Nb/ZrO_2 after evacuation at 473 K.

temperature to ~100 K can cause a shortening of Zr–O–Zr bonds in ZrO_2 crystals resulting in an increase in the O–H bond length in the bridged hydroxyl groups on the zirconia surface. Such a change in the bond length could lead to the generation of Brønsted acidity detected by low-temperature CO adsorption. Changes in the bond length in crystals caused by a temperature decrease are described in literature [26]. In view of that, the proposed explanation of apparently contradictory results seems possible.

Table 4
Number of BAS and LAS calculated per 10 mg of the catalysts on the basis of IR bands observed after desorption of pyridine at 473 K.

Catalyst	Number of LAS $\times 10^{16}$ on 10 mg of catalyst	Number of BAS $\times 10^{16}$ on 10 mg of catalyst
ZrO_2	51	0
0.3Nb/ZrO_2	17	Traces
Nb/ZrO_2	10	Traces
Pt/ZrO_2	21	2
Pt/0.3Nb/ZrO_2	15	3
Pt/Nb/ZrO_2	6	Traces

$\varepsilon = 1.5$ μmol/cm (Lewis acid sites); $\varepsilon = 1.8$ μmol/cm (Brønsted acid sites) [19].

Bridged Zr–OH–Zr hydroxyls are characterized by the band at 3666 cm^{-1}, while linear species present a vibration at 3786 cm^{-1} on bare zirconia. NbOx loading leads to a lowering of the frequency of the latter and to the appearance of a new OH band (Nb–OH) at 3740 cm^{-1}. In the CO vibration region at low CO coverage one can see two bands at 2169 and 2196 cm^{-1} assigned to CO chemisorbed on two types of Zr^{4+} ions Lewis acid sites [27]. The third band at 2152 cm^{-1} originates from H–bonding interaction of CO with 'acidic' surface OH groups. This statement is confirmed by the fact that under high CO pressure, i.e. when the peak at 2152 cm^{-1} is also present, a large fraction of bridged OH groups and Nb-OH is perturbed and transformed into a stronger and broader OH band centred at ~3550–3600 cm^{-1} [22] as typical of weakly H-bonded surface hydroxyls. The value of $\Delta\nu$ (OH) shown in Table 5 allows the estimation of the strength of Brønsted acid sites. It is clear that both Nb and Pt loading increases the strength of BAS.

Basicity of the samples was tested by CO_2 adsorption (doses from 0.39 to 3.10 μmol) at room temperature. The example of spectra obtained is shown in Fig. 6. Oxygen basicity leads to the formation of carbonates and hydroxyl basicity causes the generation of hydrogen-carbonates (both observed in 1700–1200 cm^{-1} region) [28]. It is clear that the former dominates on ZrO_2 and decreases with NbOx and Pt loading. CO_2 adsorption confirmed the presence of Lewis acid sites (the band at 2354 cm^{-1} comes from CO_2–LAS complex).

The two test reactions applied in this study allowed better insight into the acid–base properties of the samples prepared. Acetonylacetone (AcAc) cyclization is a test for Brønsted acidity and basicity [29,30]. The results obtained are summarized in Table 6. Acetonylacetone transforms primarily into two different products. In the presence of acid centres 2,5-dimethylfuran (DMF) is formed, whereas basic centres lead to the formation of 3-methyl-2-cyclopentenone (MCP). If the acid centres dominate on a catalyst surface, the selectivity ratio MCP/DMF is <1. MCP/DMF > 1 indicates the prevalence of basic centres on the surface [29]. When MCP/DMF ~ 1, one can conclude that the catalyst has an acid/base character.

The results collected in Table 6 show that ZrO_2 exhibits a very high conversion of AcAc (85%) and mainly basicity demonstrated by 98% selectivity to MCP (MCP/DMF = 64.9). AcAc conversion drastically decreases after NbOx loading on ZrO_2 (to 12% for 0.3Nb/ZrO_2 and 7% for 1Nb/ZrO_2) and the selectivity to DMF formed on BAS increases proportionally to Nb loading. The results of this test reaction confirm the lack (or the presence of very small amounts) of accessible BAS able to activate DMF formation on pristine ZrO_2.

Dehydrogenation of isopropanol to acetone gives information on the basicity. The catalysts were tested at various temperatures. Fig. 7 exhibits the results for only one temperature, 523 K. The high basicity of pristine zirconia is demonstrated by a very high selectivity to acetone. Basicity decreases after NbOx loading and after subsequent platinum impregnation. Modification of zirconia with Nb species increases the activity and selectivity to propene (related to the total acidity).

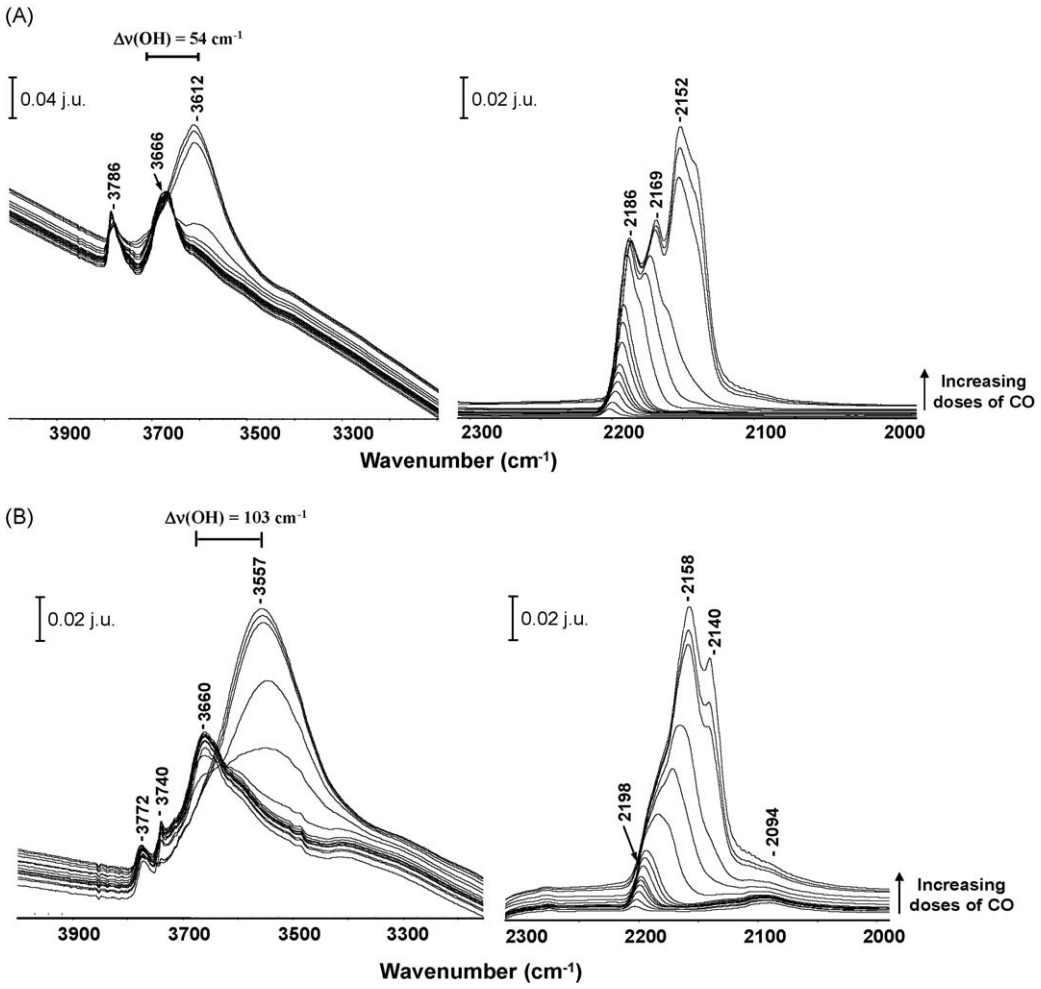

Fig. 5. CO adsorption at 77 K on ZrO_2 (A) and Pt/1Nb/ZrO_2 (B) (doses from 0.12 to 11.57 μmol).

4. Discussion

Meso–macroporous zirconia containing ca. 60% of mesopores and of the surface area of 84 m^2/g was synthesised by the sol–gel hydrothermal method and it was used as a matrix for niobium oxide species loaded as 0.3 and 1 monolayers. We had expected that these two various NbOx loadings would give rise to various acidic–basic properties of the surfaces and, as a consequence, to various catalytic properties of platinum catalysts based on such supports.

XRD patterns of meso–macroporous zirconia confirmed the presence of the tetragonal phase of ZrO_2, which was not altered after 0.3 and 1 monolayers loading of NbOx species. The presence of this phase of ZrO_2 was additionally verified by IR spectra of adsorbed CO, which indicated only one band at 2195 cm^{-1} classically assigned to CO chemisorbed on tetragonal ZrO_2 [15]. The niobium oxide phase was detected by XRD as two small bands/shoulders and the UV band at 255 nm from tetrahedrally coordinated niobium oxide. Therefore, one can postulate the presence of the NbOx phase on the ZrO_2 surface even if it is not well visible in XRD patterns, as the calcination at 673 K is expected to transform Nb-salt towards the oxide [6].

Table 5
$\Delta\nu$ (OH) for the bridged OH groups after interaction with H-bonded CO at low temperature.

Catalyst	$\Delta\nu$ (OH) (cm^{-1})
ZrO_2	54
0.3Nb/ZrO_2	83
Nb/ZrO_2	93
Pt/ZrO_2	89
Pt/0.3Nb/ZrO_2	91
Pt/Nb/ZrO_2	103

Depending on NbOx loading (0.3 or 1 monolayer) various platinum phases are generated after impregnation with H_2PtCl_6 and calcination at 673 K. Adsorption of CO combined with the FTIR study allowed us to differentiate Pt^0, Pt^+, and Pt^{2+}. The highest reduction of platinum species to Pt^0 was found on the Pt/1Nb/ZrO_2 sample. Cationic forms of platinum, both Pt^+ and Pt^{2+}, were the dominant species on Pt/0.3Nb/ZrO_2. This type of behaviour must have been caused by the highest dispersion of platinum on Pt/1Nb/ZrO_2 (highly dispersed platinum is more easily reduced) as well as by various surface properties of 0.3Nb/ZrO_2 and 1Nb/ZrO_2 supports. On the 0.3Nb/ZrO_2 support, platinum is located preferentially on the free zirconia surface in the spaces between islands built of NbOx species. Such localization has been deduced from the differing basic properties of ZrO_2, 0.3Nb/ZrO_2 and Pt/0.3Nb/ZrO_2, namely the decrease of basic sites, originating on the zirconia surface, after Pt loading (observed by the AcAc reaction). Interestingly, Pt impregnation of 1Nb/ZrO_2 leads to the growth of basic sites because platinum is loaded on NbOx. Localization of platinum species in such a 'niche' in 0.3Nb/ZrO_2 makes the agglomeration of platinum on thermal treatment much easier and consequently leads to low Pt dispersion. It also determines the surface properties of the catalysts as the Pt species are located close to the corners formed at the site of NbOx joining the surface of the zirconia support. Oxygen in such

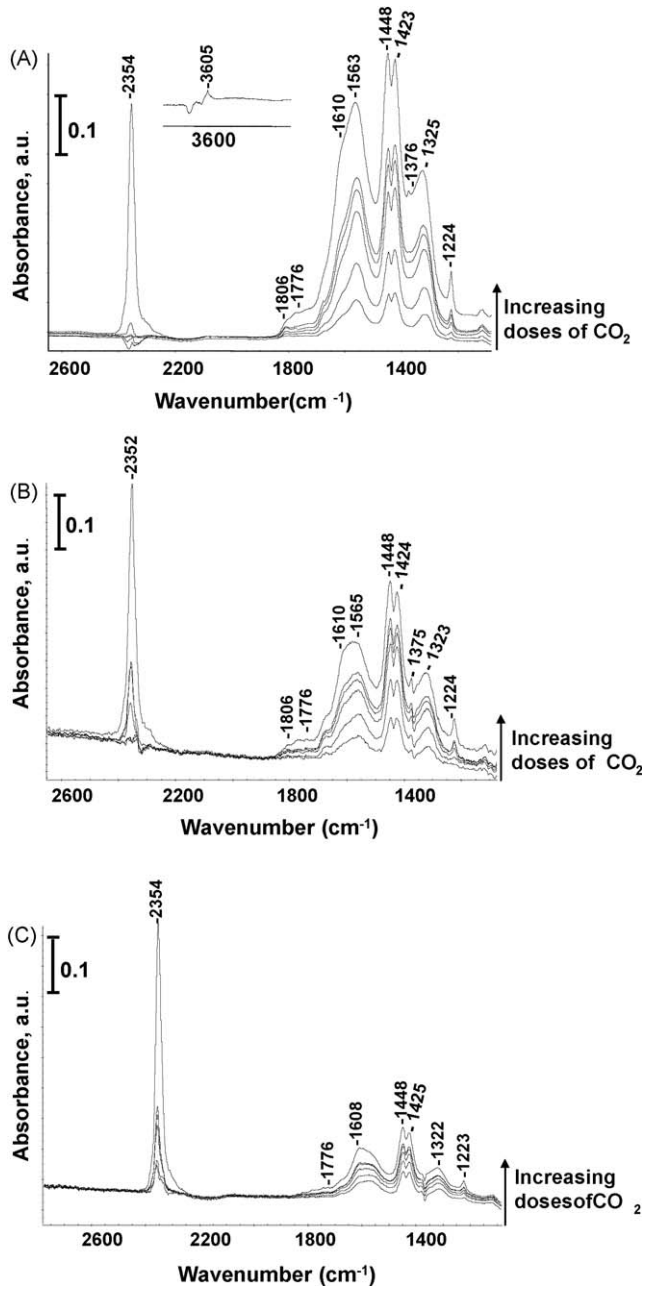

Fig. 6. CO_2 adsorption at room temperature on ZrO_2 (A), $1Nb/ZrO_2$ (B) and $Pt/1Nb/ZrO_2$ (C) (doses from 0.39 to 11.57 μmol).

Table 6
Results of acetonyloacetone (AcAc) reaction carried out at 623 K.

Catalyst	AcAc conversion (%)	DMF selectivity (%)	MCP selectivity (%)	MCP/DMF
ZrO_2	85	2	98.	49
$0.3Nb/ZrO_2$	12	27	73	2.7
$1Nb/ZrO_2$	7	93	7	0.08
Pt/ZrO_2	10	4	96	24
$Pt/0.3Nb/ZrO_2$	9	35	65	1.85
$Pt/1Nb/ZrO_2$	10	75	25	0.33

corners stabilizes the cationic platinum and therefore $Pt^{\delta+}$ is hardly reduced. This sample also presents the greater oxygen mobility, as shown by carbonate formation after CO adsorption; this favours Pt clustering upon thermal activation.

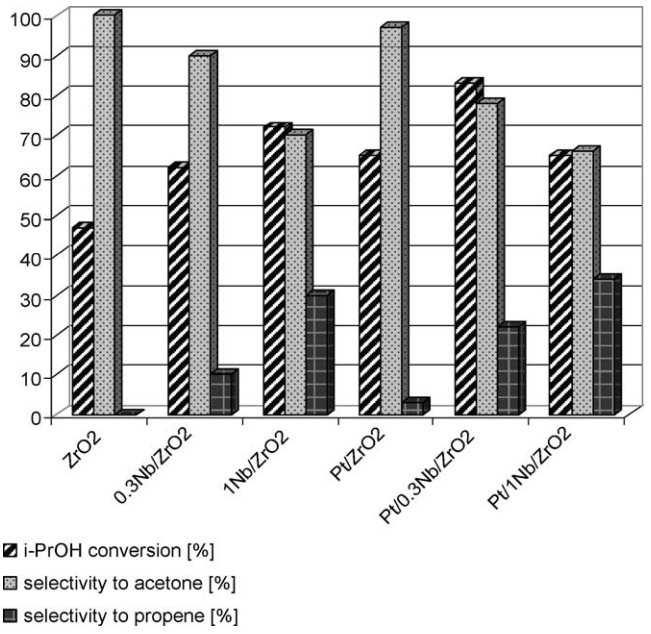

Fig. 7. The results of 2-PrOH dehydrogenation and dehydration at 523 K.

Acidic–basic properties of the prepared catalysts were measured by the use of complementary methods such as the FTIR study combined with the adsorption of probe molecules (pyridine, CO and CO_2) and test reactions (dehydration/dehydrogenation of isopropanol—i-PrOH, and cyclization of acetonylacetone—AcAc). Pyridine tested Lewis and Brønsted acidities (LAS and BAS) and for the same purpose the low-temperature (∼100 K) adsorption of CO was used, whereas CO_2 adsorption probed Lewis and hydroxyl basicities. AcAc transformation occurs on Brønsted acid and basic centres and 2-PrOH decomposition allows the detection of Lewis basicity as well as BAS/LAS.

The results of the test reaction (AcAc) and study of the adsorption of pyridine followed by FTIR clearly indicate the difference in acid–base properties depending on NbOx loading. Pure zirconia exhibits basicity ($OH^{\delta-}$) estimated from the MCP/DMF ratio in acetonylacetone cyclization and CO_2 adsorption. Moreover, Lewis acid centres are present on its surface (pyridine, CO adsorption at RT and 100 K).

Introduction of NbOx species on the zirconia surface reduces the number of LAS because of the chemical interaction of zirconia Lewis acid sites and NbOx entities. Moreover, changes in the MCP/DMF ratio result from the reduction of Brønsted basicity. These effects increase with NbOx loading. That finding suggests that NbOx species are located near both basic sites ($OH^{\delta-}$) and Lewis acid sites which chemically interact with niobium species. Such chemical interaction not only reduces the effectiveness of basic sites and LAS activity on ZrO_2 but also activates NbOx species at the site where it is linking with the zirconia support. This phenomenon is particularly well observed on $0.3Nb/ZrO_2$ by carbonate (IR bands in 1560–1300 cm^{-1} region) and hydrogen-carbonate (1610, 1448 and 1223 cm^{-1}) formation after CO and CO_2 adsorption at RT. Carbonates from CO adsorption are generated by involvement with active oxygen from NbOx species linked with ZrO_2, whereas the formation of hydrogen-carbonates from carbonates requires the presence of basic hydroxyl groups from the zirconia surface. After CO adsorption, carbonates are not formed on pure ZrO_2 and they are only slightly visible on $1Nb/ZrO_2$. Zirconia does not have centres containing active oxygen necessary for carbonate formation. Active oxygen appears in the corners formed between NbOx crystallites and the zirconia support. A monolayer of NbOx on ZrO_2

eliminates, or significantly reduces the number of corners formed at these sites. It explains the fact that a very low concentration of carbonates was formed upon CO adsorption on $1Nb/ZrO_2$. Further generation of hydrogen-carbonates observed on $1Nb/ZrO_2$ suggests that some number of basic OH groups from ZrO_2 are not totally covered by the NbOx monolayer.

Contrarily, to the phenomena of CO adsorption, CO_2 adsorption gives rise to the highest formation of carbonates and hydrogen-carbonates on pure zirconia, which exhibits the highest basicity (proved also by i-PrOH and AcAc test reactions). NbOx loading decreases the basicity. The generation of carbonates from CO_2 requires one basic oxygen from the catalyst surface, whereas when CO is adsorbed two active oxygen atoms from the surface are involved in the formation of carbonates. Such pairs of active oxygen are therefore at the above-mentioned corners on $0.3Nb/ZrO_2$.

It is worthwhile to stress that Lewis acidity of $1Nb/ZrO_2$ found by pyridine adsorption most probably partially originates from NbOx species, because niobium oxides are materials known to exhibit Lewis acidity [5]. Because BAS were not detected on ZrO_2 by pyridine adsorption we have to consider whether Brønsted acidity is created by NbOx species. However, weak Brønsted acidity of the pristine zirconia was found after CO adsorption at low temperature. In such conditions CO is weakly hydrogen bonded to bridged Zr–OH–Zr hydroxyls. The strength of BAS increases with NbOx loading and it can be partially caused by the interaction of OH groups from NbOx species with CO. It is also possible that the presence of NbOx on zirconia increases the strength of bridged OH groups.

Various surface properties of $0.3Nb/ZrO_2$ and $1Nb/ZrO_2$ indicated above have an important impact on the catalytic properties of platinum grafted on both supports. As we have indicated above, the oxidation state of platinum strongly depends on the nature of the supports used in this work. Niobium oxide is well known as a strong metal–support interaction agent [9]. Such interaction easily leads to the reduction of cationic platinum towards metallic Pt. Therefore, a monolayer of NbOx on ZrO_2 leads to the highest Pt^0 concentration. Interestingly, on the $Pt/0.3Nb/ZrO_2$ sample the dominant species is Pt^{2+} with the absence of Pt^0, which can be explained by the stabilization of Pt^{2+}–O^{2-} in the corners between NbOx species and ZrO_2 surface. Such stabilization requires the interaction with LAS and therefore Pt loading reduces Lewis acidity. Zirconia treatment with chloroplatinic acid generates weak BAS and therefore Brønsted acidity increases after Pt loading on pure ZrO_2 and zirconia not fully covered by NbOx ($0.3Nb/ZrO_2$).

5. Conclusions

Tetragonal zirconia prepared within this work is a highly basic material exhibiting both oxygen and hydroxyl basic sites. Moreover, it has Lewis acid centres and very weak BAS (bridged hydroxyls). NbOx loading decreases the basicity and the Lewis acidity and leads to the growth of BAS. Deposition of a 0.3 monolayer of NbOx on zirconia produces a very attractive material in which active oxygen atoms are located in the corners formed at the junctions between the two phases (NbOx and ZrO_2). Platinum located near these corners is stabilized in cationic form and it is easily agglomerated. Therefore, the Pt dispersion on $0.3Nb/ZrO_2$ support is the lowest measured over these materials. The highest dispersion of platinum was reached on $1Nb/ZrO_2$ due to the strong metal–support interaction (SMSI) between NbOx and Pt species. Pt loaded on $0.3Nb/ZrO_2$ increases BAS and decreases Lewis acidity stressing the role of the corners between NbOx and ZrO_2. Pt loaded on $1Nb/ZrO_2$ increases basicity.

The catalysts prepared and characterized within this work are very attractive for the Water Gas Shift reaction, catalytic properties being correlated to the aforementioned surface properties [to be published].

Acknowledgements

Polish Ministry of Science and Higher Education (grant N N204 3735 33) and CBMM (Brazil) are acknowledged for the financial support and for supplying Nb source, respectively.

References

[1] J. Goscianska, M. Ziolek, Catal. Today 137 (2008) 197.
[2] J. Goscianska, M. Ziolek, Stud. Surf. Sci. Catal. 170 B (2007) 1870.
[3] Z.Y. Yuan, A. Vantomme, A. Leonard, B.-L. Su, Chem. Commun. (2003) 1558.
[4] H.L. Tidahy, S. Siffert, J.-F. Lamonier, E.A. Zhilinskaya, A. Aboukais, Z.-Y. Yuan, A. Vantomme, B.-L. Su, X. Canet, G. De Weireld, M. Frere, T.B. N'Guyen, J.-M. Giraudon, G. Leclerq, Appl. Catal. A: Gen. 310 (2006) 61.
[5] I. Nowak, M. Ziolek, Chem. Rev. 99 (1999) 3603.
[6] M. Ziolek, Catal. Today 78 (2003) 47.
[7] J. Datka, A.M. Turek, J.M. Jehng, I.E. Wachs, J. Catal. 135 (1992) 186.
[8] T. Onfroy, G. Clet, M. Houalla, Micropor. Mesopor. Mater. 82 (2005) 99.
[9] T. Onfroy, G. Clet, M. Houalla, J. Phys. Chem. B 109 (2005) 14588.
[10] S.-C. Shen, S. Kawi, Appl. Catal. B: Environ. 45 (2003) 63.
[11] L.F. Chen, X.L. Zhou, L.E. Norena, J.A. Wang, J. Navarrete, P. Salas, A. Montoya, P. Del Angel, J. Solid State Chem. 180 (2007) 2958.
[12] E. Rodriguez-Castellon, A. Jimenes-Lopez, P. Marireles-Torres, D.J. Jones, J. Roziere, M. Trombetta, G. Busca, M. Lenarda, L. Storaro, J. Solid State Chem. 175 (2003) 159.
[13] B. Kilos, A. Tuel, M. Ziolek, J.C. Volta, Catal. Today 118 (2006) 416.
[14] X. Gao, I.E. Wachs, M.S. Wong, J.Y. Ying, J. Catal. 203 (2001) 18.
[15] K. Hadjiivanov, G. Vayssilov, Adv. Catal. 47 (2002) 307.
[16] F. Pompeo, D. Gazzoli, N.N. Nichio, Mater. Lett. 63 (2009) 477.
[17] W.Y. Guo, J. Sun, J.S. Wu, Mater. Chem. Phys. 113 (2009) 816.
[18] V. Boffa, J.E. ten Elshof, R. Garcia, D.H.A. Blank, Micropor. Mesopor. Mater. 118 (2009) 202.
[19] V. Perrichon, L. Retailleau, P. Bazin, M. Daturi, J.C. Lavalley, Appl. Catal. A: Gen. 260 (2004) 1.
[20] G. Busca, G. Phys. Chem. Chem. Phys. 1 (1999) 723.
[21] S. Khabtou, T. Chevreau, J.C. Lavalley, Micropor. Mater. 3 (1994) 133.
[22] C. Morterra, G. Cerrato, S. Di Ciero, Appl. Surf. Sci. 126 (1998) 107.
[23] C. Morterra, G. Cerrato, V. Bolis, S. Di Ciero, M. Signoretto, J. Chem. Soc., Faraday Trans. 93 (1997) 1179.
[24] A. Vimont, H. Leclerc, F. Maugé, M. Daturi, J.-C. Lavalley, S. Surblé, C. Serre, G. Férey, J. Phys. Chem. C 111 (2007) 383.
[25] A. Vimont, J.-C. Lavalley, L. Francke, A. Demourgues, A. Tressaud, M. Daturi, J. Phys. Chem. B 108 (2004) 3246.
[26] A. Katrusiak, M. Szafranski, J. Am. Chem. Soc. 128 (2006) 15775.
[27] M. Daturi, C. Binet, J.-C. Lavalley, A. Galtayries, R. Sporken, Phys. Chem. Chem. Phys. 1 (1999) 5717.
[28] V. Bolis, G. Magnacca, G. Cerrato, C. Morterra, Thermochim. Acta 379 (2001) 147.
[29] R.M. Dessau, Zeolites 10 (1990) 205.
[30] J.J. Alcaraz, B.J. Arena, R.D. Gillespie, J.S. Holmgren, Catal. Today 43 (1998) 89.